NeuroImage xxx (2014) xxx–xxx

Contents lists available at ScienceDirect

NeuroImage

journal homepage: www.elsevier.com/locate/ynimg

Bringing CLARITY to gray matter atrophy

Rory D. Spence [a], Florian Kurth [a], Noriko Itoh [b], Chandler R.L. Mongerson [a], Shannon H. Wailes [a], Mavis S. Peng [b], Allan J. MacKenzie-Graham [a,*]

[a] Ahmanson-Lovelace Brain Mapping Center, Department of Neurology, University of California, Los Angeles, Los Angeles, CA, USA
[b] Multiple Sclerosis Program, Department of Neurology, University of California, Los Angeles, Los Angeles, CA, USA

ARTICLE INFO

Article history:
Accepted 10 July 2014
Available online xxxx

ABSTRACT

Gray matter atrophy has been shown to be a strong correlate to clinical disability in multiple sclerosis (MS) and its most commonly used animal model, experimental autoimmune encephalomyelitis (EAE). However, the relationship between gray mater atrophy and the spinal cord pathology often observed in EAE has never been established. Here EAE was induced in Thy1.1-YFP mice and their brains imaged using *in vivo* magnetic resonance imaging (MRI). The brains and spinal cords were subsequently optically cleared using Clear Lipid-exchanged Acrylamide-hybridized Rigid Imaging-compatible Tissue-hYdrogel (CLARITY). Axons were followed 5 mm longitudinally in three dimensions in intact spinal cords revealing that 61% of the axons exhibited a mean of 22 axonal ovoids and 8% of the axons terminating in axonal end bulbs. In the cerebral cortex, we observed a decrease in the mean number of layer V pyramidal neurons and a decrease in the mean length of the apical dendrites of the remaining neurons, compared to healthy controls. MRI analysis demonstrated decreased cortical volumes in EAE. Cross-modality correlations revealed a direct relationship between cortical volume loss and axonal end bulb number in the spinal cord, but not ovoid number. This is the first report of the use of CLARITY in an animal model of disease and the first report of the use of both CLARITY and MRI.

Introduction

Multiple sclerosis (MS) is a putative autoimmune demyelinating disease with a neurodegenerative component whose target organ is the brain and spinal cord. Progressive gray matter atrophy is a well documented feature of MS and is widely considered as a marker of irreversible tissue damage (Chard and Miller, 2009; Charil et al., 2007; Pirko et al., 2007). Quantitative magnetic resonance imaging (MRI) studies indicate that gray matter atrophy occurs even in the earliest stages of disease (Calabrese et al., 2007; Dalton et al., 2004; De Stefano et al., 2003) and is more closely related to physical disability and cognitive impairment than either T2 or T1 white matter lesion volume (Amato et al., 2004; Chard et al., 2002; Sailer et al., 2003; Sanfilipo et al., 2006). Indeed, it is now considered to be one of the most relevant markers of permanent disability in MS (Bermel and Bakshi, 2006; Fisher et al., 2002; van den Elskamp et al., 2010).

More than a decade ago, Ferguson demonstrated axonal ovoids as the result of axonal dysfunction or injury (Ferguson et al., 1997) and Trapp further showed axonal end bulbs and axonal transection in MS lesions in the brain (Trapp et al., 1998), highlighting that axonal injury and loss are important components of MS pathology. However, it is unknown if there is a relationship between gray matter atrophy and axonal injury and transection. These questions cannot be answered in patients with MS, but they can be addressed in the most widely used mouse model of MS, experimental autoimmune encephalomyelitis (EAE).

EAE has been used extensively to understand immune and neurodegenerative mechanisms in MS. Gray matter atrophy in both the cerebellum and cerebral cortex has been observed in MS (De Stefano et al., 2003; Edwards et al., 1999; Iannucci et al., 1999; Sailer et al., 2003) and has recently been reported *in vivo* in EAE (MacKenzie-Graham et al., 2009, 2012). Cerebellar and cerebral cortex atrophy were found to correlate strongly with Purkinje cell (MacKenzie-Graham et al., 2009) and cortical neuron number (MacKenzie-Graham et al., 2012) respectively, suggesting that gray matter atrophy is closely related to neuronal loss. Furthermore, seminal work has demonstrated inflammation, demyelination, neuronal, and axonal loss in the spinal cord (Bannerman et al., 2005; Cross et al., 1993; Pender, 1987; Wujek et al., 2002) and more recently in the brain (MacKenzie-Graham et al., 2009; Mangiardi et al., 2011; Zhu et al., 2003; Ziehn et al., 2010), a recapitulation of many findings in MS (Bo et al., 2003; Peterson et al., 2001; Trapp et al., 1998). However, all of these observations are based on sparse sampling of the brain and spinal cord, not a complete evaluation of these processes throughout the entire CNS. The ability to evaluate these measures in

* Corresponding author at: Department of Neurology, David Geffen School of Medicine at UCLA, 710 Westwood Plaza, Los Angeles, CA 90095, USA.
E-mail address: amg@ucla.edu (A.J. MacKenzie-Graham).

http://dx.doi.org/10.1016/j.neuroimage.2014.07.017

three dimensions (3D) across an intact CNS would provide unique insights into relationships between these processes during disease.

Tissues are opaque to conventional light microscopy due primarily to light scattering by lipids (Chung et al., 2013; Susaki et al., 2014). In order to permit microscopic imaging of intact preparations, several techniques for the optical clearing of tissue have recently been developed. One of the earliest optical clearing methods developed used a mixture of benzyl alcohol and benzyl benzoate (BABB) to match the refractive index of fixed tissue (Dodt et al., 2007). This approach yielded only partial clearing of myelinated tissues and the clearing solutions led to the rapid loss of fluorescent signals (Erturk et al., 2012a). Nonetheless, the use of organic solvents for refractive index matching has produced very fast optical clearing times. 3D Imaging of Solvent Cleared Organs (3DISCO) can clear a brain in approximately 1 day (Erturk et al., 2012a), however, the half-life of the fluorescent signal is 1–2 days and YFP is particularly unstable in the final clearing solution. Scale uses a water-based clearing solution that preserves fluorescent signals, but requires long incubation times (weeks to months) and yields incomplete tissue clearing (Hama et al., 2011). SeeDB makes use of a hydrophilic optical clearing solution containing fructose and thiols to achieve rapid tissue clearing (3 days), but, like Scale, does not yield complete clearing of adult brain tissues (Ke et al., 2013).

Clear Lipid-exchanged Acrylamide-hybridized Rigid Imaging-compatible Tissue-hYdrogel or CLARITY is a recently developed optical clearing technology that permits intact imaging of the entire brain with minimal protein loss while preserving native fluorescence (Chung et al., 2013; Tomer et al., 2014). The CLARITY protocol calls for aggressively removing lipids by electrophoresis, leading to a clearing time of approximately 10 days. However, this requires the use of specialized electrophoresis devices that must be operated within a narrow range of parameters to yield meaningful results. The replacement of the electrophoretic tissue clearing step with passive diffusion permits for greater scalability and improved reproducibility, albeit at the cost of longer incubation times (Tomer et al., 2014).

The purpose of this study was to examine the relationship between gray matter atrophy, as visualized by MRI, and axonal integrity, as visualized by CLARITY. Here, EAE was induced in Thy1-YFP^{+} mice and *in vivo* MRI was collected followed by optical clearing of both brains and spinal cords using the "passive clearing" CLARITY technique.

Materials and methods

Overview

EAE was induced in Thy1.1-YFP^{+} C57BL/6 mice and typical clinical disease was observed, with signs beginning at day 12 and a mean peak score of 4.1 at day 21 (Fig. 1). *In vivo* MRIs were collected from five mice with EAE 25 days after disease induction and from six age- and sex-matched healthy controls. The mice were then sacrificed, CLARITY performed on their CNS, and 3D confocal images collected.

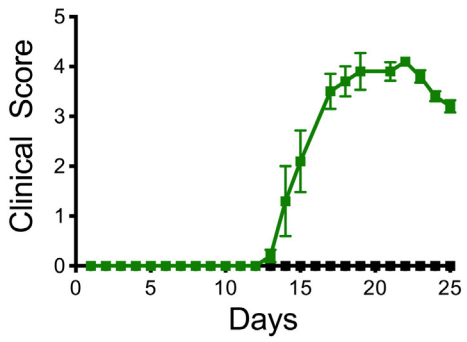

Fig. 1. Experimental autoimmune encephalomyelitis. Graph of the mean clinical disease score in EAE (green) and healthy control (black) mice plotted against disease duration. Mean peak disease reached a score of 4.1 at day 21.

Animals

Male B6.Cg-Tg(Thy1-YFP)HJrs/J mice (Jackson Laboratories, Bar Harbor, ME) between 8 and 10 weeks of age were used for all experiments. Mice were maintained in a 12 h dark/light cycle with access to food and water *ad libitum*. All procedures were performed in accordance to the guidelines of the National Institutes of Health and the Chancellor's Animal Research Committee of the University of California, Los Angeles Office for the Protection of Research Subjects.

Experimental autoimmune encephalomyelitis

Mice were immunized s.c. with MOG peptide 35–55 (300 μg/mouse) and *Mycobacterium tuberculosis* (500 μg/mouse) emulsified in complete Freund's adjuvant, in a volume of 0.1 ml/mouse over the right-draining inguinal and axillary lymph nodes. One week later a booster immunization was delivered s.c. over the contralateral lymph nodes. Pertussis toxin (500 ng/mouse; List Biological Laboratories, Campbell, CA) was injected intraperitoneally on days 0 and 2 (Liu et al., 2003; Suen et al., 1997). EAE was graded on a scale of 0–5, based on difficulty with ambulation (Pettinelli and McFarlin, 1981).

MRI acquisition

Mice were anesthetized with isoflurane and their heads secured with bite and ear bars. Respiration rate was monitored and the mice were maintained at 37 °C using a circulating water pump. *In vivo* magnetic resonance imaging was performed using a 200 mm horizontal bore 7.0 T Bruker imaging spectrometer with a micro-imaging gradient insert with a maximum gradient strength of 100 G/cm and 30 mm birdcage RF coil (Bruker Instruments, Billerica, MA). An actively decoupled quadrature surface coil array was used for signal reception and a 72-mm birdcage coil was used for transmission. Images were acquired and reconstructed using ParaVision 5.1 software. Imaging parameters were as follows: rapid-acquisition with relaxation enhancement (RARE) sequence, matrix dimensions = 256 × 128 × 64; field of view = 3.84 cm × 1.92 cm × 0.96 cm; repetition time (TR) = 3500 ms; apparent time to echo (apparent TE) = 32 ms; echo train length = 16; and total scan time = 37 min. Spatial resolution was 150 μm^3 per voxel.

MRI analysis

Images were skull-stripped using the Brain Surface Extractor (BSE) and residual non-brain signal was removed by a single operator (RDS) manually editing the masks using BrainSuite 11a (Shattuck and Leahy, 2001) and bias-field inhomogeneities were removed using the N3 correction. After inhomogeneity correction, a minimum deformation atlas (MDA) was produced as described (MacKenzie-Graham et al., 2009). Images were aligned to the MDA using Alignlinear (AIR) (Woods et al., 1998a,b) to permit the direct comparison of images in a standard space, correcting both gross size differences and gross intensity differences, yet preserving anatomically significant local changes that a non-linear warp may erase. Following creation of this atlas, cerebral cortices were manually labeled on the atlas. The labels were then warped onto the individual spatially normalized images and manually corrected by a single operator (AMG) to produce standardized estimates of gray matter volumes in individual subjects. An intensity rescaling cost function was used in order to intensity-normalize the images. All automated image processing was performed using the LONI Pipeline Processing Environment (Rex et al., 2003) on an 8-processor core Mac Pro computer (Apple, Cupertino, CA).

Please cite this article as: Spence, R.D., et al., Bringing CLARITY to gray matter atrophy, NeuroImage (2014), http://dx.doi.org/10.1016/j.neuroimage.2014.07.017

Cerebral cortex labels were based on the Mouse Atlas Project 2003 mouse brain atlas (MacKenzie-Graham et al., 2004). For clarity and consistency, our cerebral cortex label was bounded ventrally by the plane inferior to the most anterior point of the corpus callosum at midline. Importantly, this label contained the somatosensory regions (primary and secondary) and the motor cortex (primary and secondary) (MacKenzie-Graham et al., 2012). Additional anatomical information was obtained from the Franklin and Paxinos mouse brain atlas (Franklin and Paxinos, 2008).

To determine the reproducibility of our *in vivo* MRI data, 10 wild-type female C57BL/6J mice were scanned *in vivo* and brain volumes were measured. The average brain volume was 436 mm^3 with a standard error of 2.3 mm^3 (95% confidence interval, 432–440; data not shown). To establish scan–rescan reliability a single wild-type female C57BL/6J mouse was imaged *in vivo* four times on separate days. The average brain volume was 438 mm^3 with a standard error of 1.8 mm^3 (95% confidence interval, 434–442; data not shown).

CLARITY

All tissue were optically cleared using the CLARITY protocol (Chung et al., 2013) (http://clarityresourcecenter.org/) modified for "passive clearing" (Tomer et al., 2014). Briefly, EAE and healthy control mice were anesthetized and perfused with 25 ml of ice cold 0.1 M PBS followed by 25 ml of ice cold hydrogel. Each brain and spinal cord were quickly dissected and placed in 20 ml of cold hydrogel in a 50 ml conical tube for 48 h at 4 °C. After 48 h the 50 ml tube lids were twisted open, yet not removed, and placed in a desiccation chamber (McMaster-Carr, Santa Fe Springs, CA). The desiccation chamber was then attached to a vacuum for 10 min to allow for a negative pressure to form inside. Immediately after the 10 min the chamber was purged with nitrogen gas. The desiccation chamber lid was removed and the 50 ml tube lid was quickly screwed shut to prevent exposure to the outside air. The 50 ml tubes were then placed in a 37 °C water bath for 4–5 h to allow for adequate polymerization of the hydrogel and tissue. After the hydrogel was polymerized, excess gel was removed by placing the tissue in a kimwipe (Kimberly-Clark, Neenah, WI) and gently rubbing. The whole brain was then cut sagittally down the midline to generate two hemispheres. Both hemispheres were placed into one 50 ml tube with clearing solution (200 mM boric acid, 4% SDS, pH 8.5) and placed in an incubator with agitation at 37 °C. Each spinal cord was placed into its own 50 ml tube. Every 24 h the clearing solution was replaced with fresh clearing solution until the tissue had completely cleared. This process relies entirely on passive diffusion to remove all lipids from the tissue, the incubation time required was substantial: 5 weeks for the brain and 3 weeks for the spinal cord. This process, known as "passive clearing" (Tomer et al., 2014) was used instead of electrophoretic clearing (Chung et al., 2013). Passive clearing does not require dedicated electrophoretic equipment and can easily be scaled to allow complete clearing of all brains and spinal cords simultaneously with high reproducibility and low variation between subjects. Once clear, tissue was submerged in FocusClear (CelExplorer Labs, Hsinchu, Taiwan) for 24 h at 37 °C to allow for refractive index matching. Tissue was then placed in a 35 mm glass bottom dish (Ted Pella, Redding CA) with a thin barrier of BluTack putty (Bostick, Fort Wayne, IN) around the tissue to prevent tissue and FocusClear from moving. Tissue was then immediately used for microscopy.

Microscopy

Confocal laser scanning microscopy was performed at the CNSI Advanced Light Microscopy/Spectroscopy Shared Resource Facility at UCLA. A Leica TCS-SP5 AOBS confocal microscope was used in combination with Leica Application Suite Advanced Fluorescence (LAS AF) software (Leica Microsystems, Inc., Buffalo Grove, IL). The resonant scanner was used at a speed of 8000 Hz. 5× images of the spinal cord and cerebral cortex were taken with a resolution of 512 × 512 and a line average of 8. The 5× objective used was a Lecia HC PL FLUOTAR with an NA of 0.15. The dimensions of each voxel were 1.5 μm × 1.5 μm × 44.31 μm. 10× images of the spinal cord and cerebral cortex were taken with a

Fig. 2. Thy1-YFP expression in the spinal cord. A 3D image stack of Thy1-YFP expression in intact cervical and thoracic spinal cord in a healthy control (CON) (A) and an EAE mouse (B) imaged at 5× with a pixel resolution of 1.5 μm × 1.5 μm × 44.31 μm. (C) Total spinal cord (SP) Thy1-YFP expression was measured in a 10 mm long spinal cord. EAE mice demonstrated a statistically significant reduction of 20% in spinal cord Thy1-YFP expression compared to healthy controls. n = 5. *p = 0.0099. *T*-test analysis. Error bars indicate SEM.

Please cite this article as: Spence, R.D., et al., Bringing CLARITY to gray matter atrophy, NeuroImage (2014), http://dx.doi.org/10.1016/j.neuroimage.2014.07.017

resolution of 512 × 512 and a line average of 8. The 10× objective used was a Leica HCX PL FLUOTAR with an NA of 0.3. The dimensions of each voxel were 760 nm × 760 nm × 11.02 μm. All images were captured using the same acquisition parameters, specifically exposure time. LAS AF stitched the images together to form large high-resolution images. Vaa3D64 was used to make to make bitmap still frames of image stacks (http://penglab.janelia.org). MPEG Streamclip was used to make mp4 movies from the bitmap still frames (http://www.squared5.com).

CLARITY analysis

To measure the total Thy1-YFP expression in the spinal cord and cerebral cortex, individual 5× images were manually outlined in ImageJ (http://rsbweb.nih.gov/ij/) by a single operator (RDS). Images were then converted to greyscale and set to a universal threshold for all subjects. Percent expression was then measured in each outlined image. The number of ovoid positive axons was measured by randomly choosing 25 axons that had a contiguous length of at least 5 mm from our 5× images. An axon was considered ovoid positive if it had at least one ovoid along its length. The number of ovoids per axon was measured by choosing 25 ovoid positive axons that had a contiguous length of at least 5 mm. The number of ovoids present on each axon was then manually counted. The number of axons that terminated in end bulbs was measured by randomly choosing 25 axons from the dorsal corticospinal tract. An axon was considered end bulb positive if it ended in a swollen bulb and had no other visible connection. The number of cortical layer V pyramidal neurons was counted in 5× images of an entire hemisphere of the brain. For clarity and consistency, the cerebral cortex boundaries were the same as those used in MRI, bounded ventrally by the plane inferior to the most anterior point of the corpus callosum at midline. Importantly, this label contained somatosensory (primary and secondary) and motor cortex (primary and secondary) (MacKenzie-Graham et al., 2012). This area was outlined in each image of the 3D stacks and then converted to greyscale. Images were then set to a universal threshold for all subjects. The Image-based Tool for Counting Nuclei (ITCN; http://rsb.info.nih.gov/ij/plugins/itcn.html) plugin was then used to count only the somas of layer V pyramidal neurons. Dendrite length was measured in layer V pyramidal neurons in the somatosensory and motor cortices by randomly choosing 25 neurons and manually tracing the dendrites in three dimensions from the soma to their most distal extent near the dorsal surface of the cortex in ImageJ from our 10× images.

Statistical analysis

MRI and CLARITY data were analyzed using a Welch's *t*-test. Regression analysis was also performed and significance was determined at the 95% confidence interval. All statistical analyses were performed using Prism 6 software (Graphpad, La Jolla, CA).

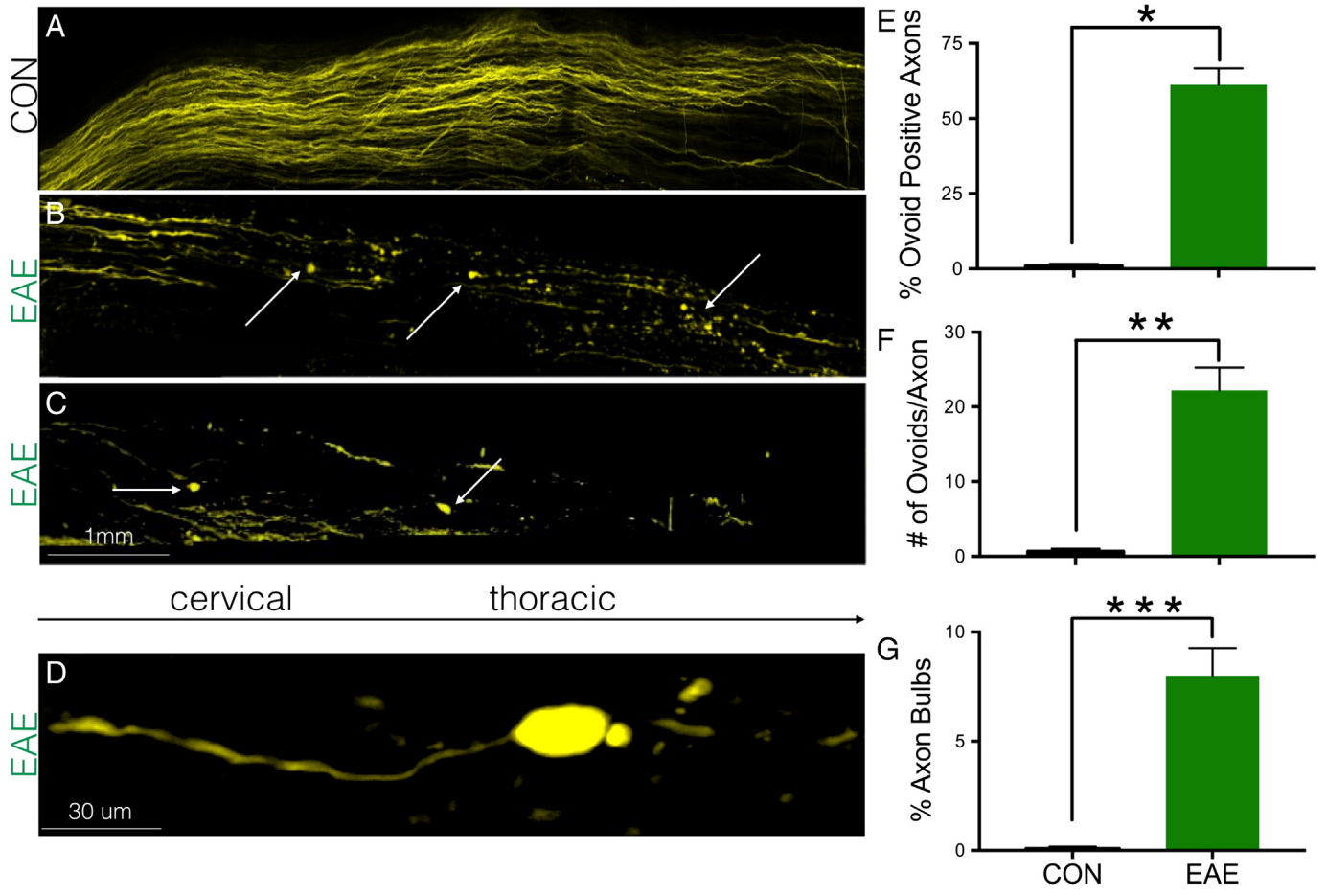

Fig. 3. Spinal cord pathology. Lateral view of a 3D image stack of the dorsal corticospinal tract from cervical to thoracic segments from a healthy control (CON) (A) and an EAE mouse (B/C). Note the absence of axonal ovoids in the healthy control compared to the EAE mouse (arrows). (C/D) Dorsal corticospinal tract Thy1-YFP^{+} axons ended in axonal bulbs in the EAE mouse (arrows). (E) 61% of axons from the EAE mice had at least one ovoid on each axon. (F) Ovoid positive axons contained an average of 22 ovoids. (G) 8% of axons from the EAE mice had at least one axonal end bulb. Virtually no ovoids nor end bulbs were observed in healthy control mice. n = 5. *p = 0.0003, **p = 0.002, ***p = 0.0033. *T*-test analysis. Error bars indicate SEM.

Please cite this article as: Spence, R.D., et al., Bringing CLARITY to gray matter atrophy, NeuroImage (2014), http://dx.doi.org/10.1016/j.neuroimage.2014.07.017

Results

Axonal ovoids and end bulbs in the spinal cord

Intact 10 mm long spinal cord sections containing cervical and thoracic segments from mice with EAE and healthy controls were optically cleared using CLARITY and imaged (Figs. 2A/B, Movie 1). The total amount of Thy1-YFP expression was measured and a loss of 20% of Thy1-YFP fluorescence was observed in EAE mice compared to healthy controls (Fig. 2C) ($p = 0.0099$).

A distinguishing feature of axonal damage in both MS and EAE is the presence of axonal ovoids. These ovoids are thought to represent disruption of fast axonal transport (Koo et al., 1990; Sherriff et al., 1994) or alterations of axonal microtubules that lead to Wallerian degeneration (Erturk et al., 2007; Imitola et al., 2011). Large numbers of axonal ovoids were observed in the dorsal corticospinal tract of the optically cleared spinal cords in EAE mice (Figs. 3A–D). Since CLARITY permits the examination of pathology in intact tissue, the number of axonal ovoids in dorsal corticospinal tract axons over a 5 mm length in three dimensions was quantified. 61% of axons in the dorsal corticospinal tract exhibited ovoids in EAE mice, with virtually none present in normal controls (Fig. 3E) ($p = 0.0003$). The number of ovoids present on each ovoid positive axon was counted next. Surprisingly, ovoid positive axons contained an average of 22.2 ± 3.1 ovoids over a length of 5 mm, with some axons containing more than 60 ovoids (Fig. 3F). The number of transected axons that ended in a swollen end bulb was then measured. 8% of axons in the dorsal corticospinal tract terminated in end bulbs in EAE mice, with virtually none in healthy control mice (Fig. 3G) ($p = 0.0033$). While most ovoids appeared to be clustered near areas of axonal transection, ovoids were also present outside areas of clustering. Similarly, axonal end bulbs appeared most commonly near clusterings of ovoids. However, axonal transection was also observed outside of ovoid clusters, albeit to a lesser degree.

Cortical pathology

The observation of axonal pathology in the dorsal corticospinal tract led to the examination of cortical pathology in the same mice. Intact cerebral hemispheres from mice with EAE and healthy controls were optically cleared using CLARITY and imaged (Figs. 4A/B, Movie 2). The total amount of Thy1-YFP expression in the cerebral cortex was measured and a loss of 17% was observed in EAE mice compared to healthy controls (Fig. 4G) ($p = 0.0038$). Previous work by Porrero et al. had shown that injection of a fluorescent tracer in layer V cells of the primary motor and somatosensory cortex led to high expression of the fluorescent label in the dorsal corticospinal tract of the thoracic spinal cord, demonstrating that the axons of layer V pyramidal neurons project through the dorsal corticospinal tract (Porrero et al., 2010). Given the observation of axonal ovoids and end bulbs in the dorsal corticospinal tract in EAE, the total number of layer V Thy1-YFP$^+$ pyramidal neurons in the cerebral cortices was counted. Healthy control mice had a mean of 33,553 ± 274.9 layer V pyramidal neurons, whereas mice with EAE had a mean of 31,157 ± 605.5 (Figs. 4C/D), a difference of 7% (Fig. 4H) ($p = 0.013$).

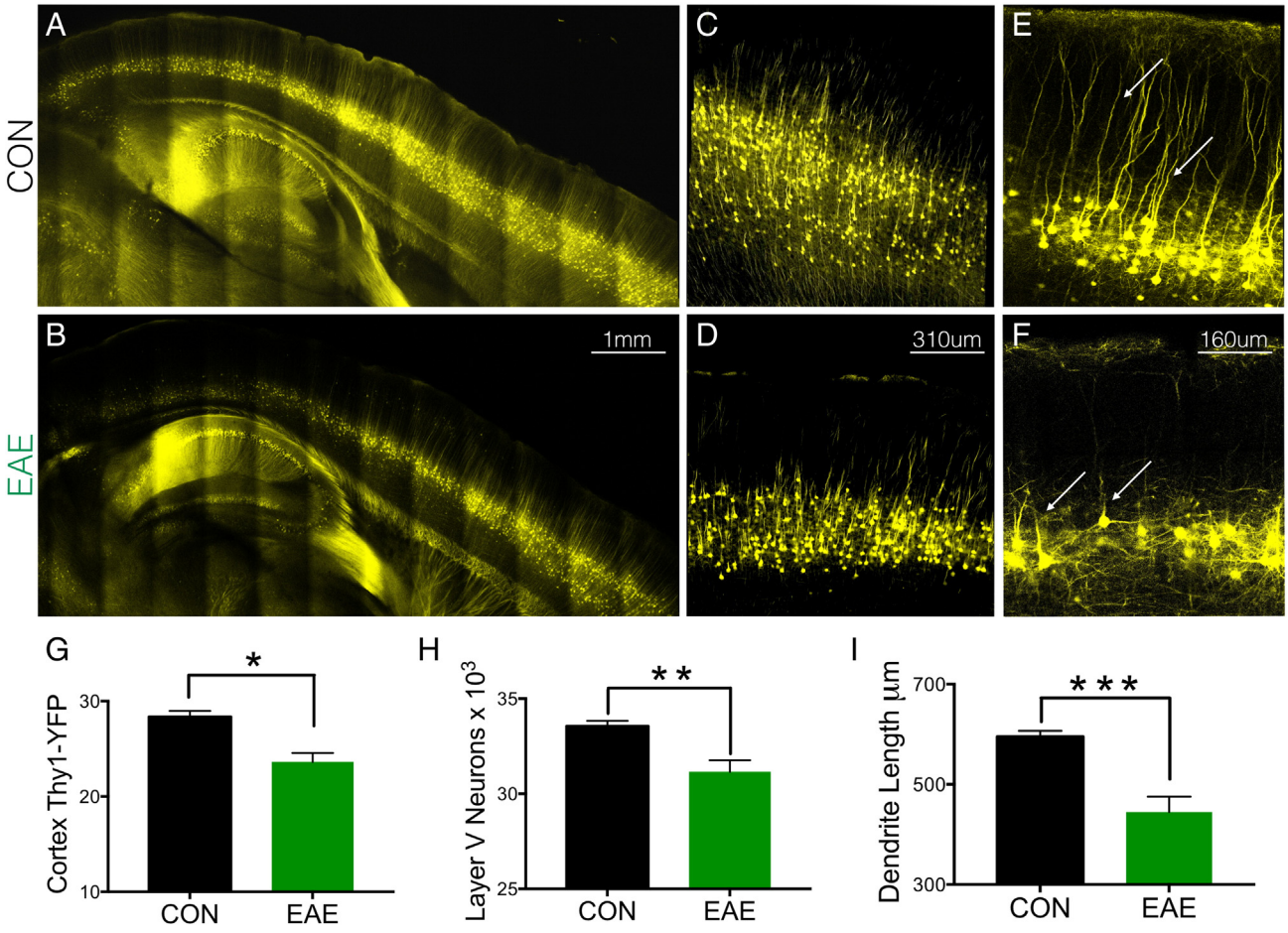

Fig. 4. Cortical pathology. A 3D image stack of Thy1-YFP$^+$ neurons in the cerebral cortex and hippocampus from healthy control (CON) (A) and EAE mice (B). Layer V pyramidal neurons in healthy control (C) and EAE mice (D). Apical dendrites (arrows) from healthy control (E) and EAE mice (F). (G) EAE mice demonstrated a 17% decrease in Thy1-YFP expression in the cerebral cortex compared to healthy control mice. (H) EAE mice demonstrated a loss of 7% of layer V pyramidal neurons compared to healthy control mice. (I) EAE mice demonstrated a decrease in dendrite length of 25% compared to healthy control mice. n = 5. *$p = 0.0038$, **$p = 0.013$, ***$p = 0.0001$. *T*-test analysis. Error bars indicate SEM.

Please cite this article as: Spence, R.D., et al., Bringing CLARITY to gray matter atrophy, NeuroImage (2014), http://dx.doi.org/10.1016/j.neuroimage.2014.07.017

In addition to an overall decrease in the number of cortical layer V pyramidal neurons, apical dendrite lengths also appeared to be decreased in the surviving neurons in EAE mice compared to healthy controls (Figs. 4E/F). The lengths of the apical dendrites of layer V pyramidal neurons in the somatosensory and motor cortices were measured in EAE mice and healthy controls. Healthy control mice had a mean apical dendrite length of 595.2 ± 11.48 um, whereas EAE mice had a mean of 444.7 ± 30.81 um, a decrease of 25% (Fig. 4I) ($p = 0.0001$).

Cortical volume loss

Prior to sacrificing the mice, *in vivo* MRI scans at day 25 of EAE were performed (Fig. 5A). Volumetry was used to determine if there were any cortical volume differences between EAE and healthy controls. The volume of the cerebral cortex in healthy control mice had a mean of 73.5 ± 0.77 mm^3 and mice with EAE had a mean of 68.3 ± 0.99 mm^3, a difference of 7% (Fig. 5B)($p = 0.0032$), consistent with our previous findings of cerebral cortical atrophy in C57BL6 mice with EAE (MacKenzie-Graham et al., 2012).

Cortical volume loss is correlated with axonal end bulbs in the spinal cord

The relationship between cortical atrophy by MRI and underlying pathology by CLARITY was determined by regression analyses performed on our *in vivo* MRI cortical volume data with our layer V pyramidal cell counts, axonal ovoid, and end bulb CLARITY data. Interestingly, a very strong direct correlation between cortical volume and cortical layer V pyramidal neuron number was observed ($R^2 = 0.83$, $p = 0.032$). Further, a very strong negative correlation between *in vivo* MRI cortical volume and axonal end bulbs in cord was also seen ($R^2 = 0.81$, $p = 0.040$). However, there was no correlation between *in vivo* MRI cortical volume and axonal ovoids in cord ($R^2 = 0.01$, $p = 0.86$). Together this showed that smaller cerebral cortex volume by MRI is directly related to permanent damage as measured by loss of layer V pyramidal cells in the cerebral cortex and axonal end bulbs in the dorsal corticospinal tract of the spinal cord.

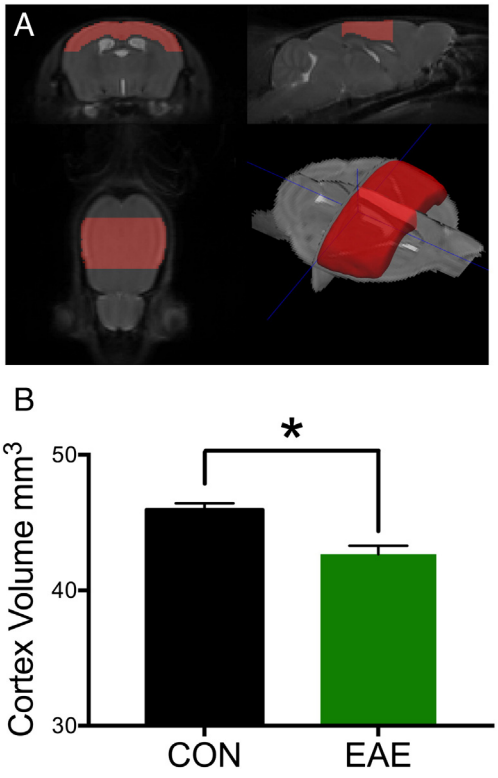

Fig. 5. Cortical volume loss in EAE. (A) A minimum deformation atlas comprising the *in vivo* MRI scans of both healthy control (CON) and EAE mice demonstrating the extent of the cerebral cortex delineation (red). (B) Cortical volume loss of 7% was seen in EAE mice *versus* healthy controls. n = 5. *p = 0.0032. *T*-test analysis. Error bars indicate SEM.

Discussion

In MS, inflammatory activity and white matter lesions are only weakly correlated with clinical disability (Brex et al., 2002). Conversely, gray matter atrophy correlates strongly with clinical disease progression (Rudick and Trapp, 2009; Vigeveno et al., 2012) and is thought to be a biomarker for neurodegeneration (Gold and Voskuhl, 2009; Vigeveno et al., 2012). To address the cellular mechanisms that drive gray matter atrophy and neurodegeneration we must go beyond MRI and use histology to observe the pathologies that underlie the changes detected by MRI.

In the last decade, MS research has focused on the role of axonal pathology and neuronal loss as the cause of permanent clinical disability, with axonal loss now accepted as a major cause of irreversible disability in MS. Axonal loss has been shown to occur in the settings of both acute inflammatory demyelination (Trapp et al., 1998) and chronic demyelination (Bjartmar et al., 2000; Lovas et al., 2000). In fact, recent animal studies have shown not only axonal loss, but also neuronal loss in the setting of inflammatory demyelination (Bannerman and Hahn, 2007; Bannerman et al., 2005; MacKenzie-Graham et al., 2009, 2012; Mangiardi et al., 2011; Ziehn et al., 2010).

Until now histological studies have focused on a sparse sampling of the tissue in question, as it was not previously possible to do a complete evaluation of these tissues 3-dimensionally throughout the entire CNS. With CLARITY, imaging cell populations in 3D in intact tissue is possible (Chung et al., 2013; Tomer et al., 2014). For example, a common pathological characteristic of axons in both MS and EAE is the presence of ovoids and end bulbs (Ferguson et al., 1997; Imitola et al., 2011; Trapp et al., 1998). Yet, despite their hypothesized importance (Ferguson et al., 1997; Imitola et al., 2011; Trapp et al., 1998), it has been difficult to fully appreciate their frequency or relationship to each other along an axon since most pathology on the spinal cord was performed on transverse sections that bisect individual axons (Bannerman and Hahn, 2007; Bannerman et al., 2005; Shriver and Dittel, 2006). Likewise, physically sectioning the spinal cord into longitudinal slices can cause data to be lost since axons will come into and out of the plane of section (Erturk and Bradke, 2013).

Erturk and colleagues demonstrated the utility of optical clearing methods for the analysis of axonal injury and regeneration. 3DISCO (3-dimensional imaging of solvent cleared organs) (Erturk et al., 2012a) permitted them to evaluate the capacity of axons to regenerate after an injury in the spinal cord by visualizing the trajectories of the regenerating axons in 3-dimensions through the spinal cord (Erturk et al., 2012b). Similarly, using CLARITY we were able to measure the number of axonal ovoids and end bulbs in axons for distances over 5 mm. Our results demonstrated that axonal ovoids and end bulbs are common in the dorsal corticospinal tract in mice with EAE. By following axons through the spinal cord we could determine the number of ovoids per axon and the number of axonal end bulbs in the dorsal corticospinal tract. Furthermore, we were able to visualize and count all Thy1-YFP^+ layer V pyramidal neurons in the cerebral cortex, not just an estimate based on counting neurons in widely-spaced serial sections. This is the underlying strength of optical clearing methods, the ability to observe phenomena in 3D that were previously only glimpsed at using physical sectioning methods in 2D.

A very recently developed approach, CUBIC (clear, unobstructed brain imaging cocktails and computational analysis), combines rapid, extensive tissue clearing with the ability to perform immunohistochemistry (Susaki et al., 2014). Future studies may benefit from the use of this promising new method, allowing the combination of inherent fluorescence with antibody probing, all in the context of an intact brain. This will permit investigators to ask more insightful questions in order to

Please cite this article as: Spence, R.D., et al., Bringing CLARITY to gray matter atrophy, NeuroImage (2014), http://dx.doi.org/10.1016/j.neuroimage.2014.07.017

more fully understand the mechanisms that underlie gray matter atrophy.

In vivo MRI in mice has become a promising and widely available technique to examine brain morphology (Bock et al., 2006; Delatour et al., 2006). Its quantitative three-dimensional format makes it an accurate tool to measure volume (Badea et al., 2007; Kovacevic et al., 2005; MacKenzie-Graham et al., 2009). MRI has permitted the repeated measure of neuroanatomical structures to evaluate the progression of volume loss in these structures over time *in vivo* (Lau et al., 2008; MacKenzie-Graham et al., 2012; Zhang et al., 2010). In MS, gray matter atrophy in the brain is measured using MRI to evaluate disease progression. Using *in vivo* MRI, we demonstrated that EAE mice had decreased cortical volumes, consistent with our previous report (MacKenzie-Graham et al., 2012). Here we used both CLARITY and *in vivo* MRI in the same experimental animals, permitting us to determine that the number of axonal end bulbs in the spinal cord is strongly correlated with the volume of cerebral cortical gray matter. Importantly, axonal ovoids in the spinal cord did not show a correlation with cerebral cortex volume, suggesting that axonal damage short of transection is insufficient to cause gray matter loss in the cortex. This is consistent with recent findings demonstrating reversible axon damage in EAE (Nikic et al., 2011). That said, it has also been postulated that the presence of axonal ovoids will eventually lead to axonal loss and Wallerian degeneration (Erturk et al., 2007; Imitola et al., 2011). Together these observations suggest that there may be a critical window whereby axons may be damaged but not yet transected. If a neuroprotective treatment were initiated within this critical window, cortical atrophy may be averted.

Conclusions

The use of both MRI and CLARITY provides a unique opportunity to explore the relationship between gray matter atrophy and the pathologies that underlie it. Here, the combination of these techniques allowed us to appreciate that there is a relationship between cortical atrophy and axonal end bulbs, but not axonal ovoids, an insight that suggests that there may be a window of reversibility in axonal damage. The combination of CLARITY with immunohistochemistry (Chung et al., 2013; Tomer et al., 2014) may permit further interrogation of the CNS in EAE to determine the extent of inflammation or demyelination or in fact any number of other processes. Most importantly, the use of both MRI and CLARITY as applied herein to EAE now sets a precedent for a novel approach to better discern neuropathological processes in intact tissues in 3D in a variety of neurodegenerative diseases.

Supplementary data to this article can be found online at http://dx.doi.org/10.1016/j.neuroimage.2014.07.017.

Acknowledgments

This work was generously supported by the National Multiple Sclerosis Society (NMSS) grant FG 1759A1/1 and the Conrad N. Hilton Foundation. We thank Dr. Laurent Bentolila and Dr. Matthew Schibler for their invaluable assistance with confocal microscopy. We thank Dr. Stephen Sawiak for developing the pulse sequence used for magnetic resonance imaging. We thank Dr. Rhonda Voskuhl for the insightful discussion and review of the manuscript. We thank those that have contributed to the CLARITY forum (http://forum.claritytechniques.org).

References

Amato, M.P., Bartolozzi, M.L., Zipoli, V., Portaccio, E., Mortilla, M., Guidi, L., Siracusa, G., Sorbi, S., Federico, A., De Stefano, N., 2004. Neocortical volume decrease in relapsing-remitting MS patients with mild cognitive impairment. Neurology 63, 89–93.

Badea, A., Ali-Sharief, A.A., Johnson, G.A., 2007. Morphometric analysis of the C57BL/6J mouse brain. Neuroimage 37, 683–693.

Bannerman, P.G., Hahn, A., 2007. Enhanced visualization of axonopathy in EAE using thy1-YFP transgenic mice. J. Neurol. Sci. 260, 23–32.

Bannerman, P.G., Hahn, A., Ramirez, S., Morley, M., Bonnemann, C., Yu, S., Zhang, G.X., Rostami, A., Pleasure, D., 2005. Motor neuron pathology in experimental autoimmune encephalomyelitis: studies in THY1-YFP transgenic mice. Brain 128, 1877–1886.

Bermel, R.A., Bakshi, R., 2006. The measurement and clinical relevance of brain atrophy in multiple sclerosis. Lancet Neurol. 5, 158–170.

Bjartmar, C., Kidd, G., Mork, S., Rudick, R., Trapp, B.D., 2000. Neurological disability correlates with spinal cord axonal loss and reduced N-acetyl aspartate in chronic multiple sclerosis patients. Ann. Neurol. 48, 893–901.

Bo, L., Vedeler, C.A., Nyland, H., Trapp, B.D., Mork, S.J., 2003. Intracortical multiple sclerosis lesions are not associated with increased lymphocyte infiltration. Mult. Scler. 9, 323–331.

Bock, N.A., Kovacevic, N., Lipina, T.V., Roder, J.C., Ackerman, S.L., Henkelman, R.M., 2006. In vivo magnetic resonance imaging and semiautomated image analysis extend the brain phenotype for cdf/cdf mice. J. Neurosci. 26, 4455–4459.

Brex, P.A., Ciccarelli, O., O'Riordan, J.I., Sailer, M., Thompson, A.J., Miller, D.H., 2002. A longitudinal study of abnormalities on MRI and disability from multiple sclerosis. N. Engl. J. Med. 346, 158–164.

Calabrese, M., Atzori, M., Bernardi, V., Morra, A., Romualdi, C., Rinaldi, L., McAuliffe, M.J., Barachino, L., Perini, P., Fischl, B., Battistin, L., Gallo, P., 2007. Cortical atrophy is relevant in multiple sclerosis at clinical onset. J. Neurol. 254, 1212–1220.

Chard, D., Miller, D., 2009. Grey matter pathology in clinically early multiple sclerosis: evidence from magnetic resonance imaging. J. Neurol. Sci. 282, 5–11.

Chard, D.T., Griffin, C.M., Parker, G.J., Kapoor, R., Thompson, A.J., Miller, D.H., 2002. Brain atrophy in clinically early relapsing-remitting multiple sclerosis. Brain 125, 327–337.

Charil, A., Dagher, A., Lerch, J.P., Zijdenbos, A.P., Worsley, K.J., Evans, A.C., 2007. Focal cortical atrophy in multiple sclerosis: relation to lesion load and disability. Neuroimage 34, 509–517.

Chung, K., Wallace, J., Kim, S.Y., Kalyanasundaram, S., Andalman, A.S., Davidson, T.J., Mirzabekov, J.J., Zalocusky, K.A., Mattis, J., Denisin, A.K., Pak, S., Bernstein, H., Ramakrishnan, C., Grosenick, L., Gradinaru, V., Deisseroth, K., 2013. Structural and molecular interrogation of intact biological systems. Nature 497, 332–337.

Cross, A.H., O'Mara, T., Raine, C.S., 1993. Chronologic localization of myelin-reactive cells in the lesions of relapsing EAE: implications for the study of multiple sclerosis. Neurology 43, 1028–1033.

Dalton, C.M., Chard, D.T., Davies, G.R., Miszkiel, K.A., Altmann, D.R., Fernando, K., Plant, G.T., Thompson, A.J., Miller, D.H., 2004. Early development of multiple sclerosis is associated with progressive grey matter atrophy in patients presenting with clinically isolated syndromes. Brain 127, 1101–1107.

De Stefano, N., Matthews, P.M., Filippi, M., Agosta, F., De Luca, M., Bartolozzi, M.L., Guidi, L., Ghezzi, A., Montanari, E., Cifelli, A., Federico, A., Smith, S.M., 2003. Evidence of early cortical atrophy in MS: relevance to white matter changes and disability. Neurology 60, 1157–1162.

Delatour, B., Guegan, M., Volk, A., Dhenain, M., 2006. In vivo MRI and histological evaluation of brain atrophy in APP/PS1 transgenic mice. Neurobiol. Aging 27, 835–847.

Dodt, H.U., Leischner, U., Schierloh, A., Jahrling, N., Mauch, C.P., Deininger, K., Deussing, J.M., Eder, M., Zieglgansberger, W., Becker, K., 2007. Ultramicroscopy: three-dimensional visualization of neuronal networks in the whole mouse brain. Nat. Methods 4, 331–336.

Edwards, S.G., Gong, Q.Y., Liu, C., Zvartau, M.E., Jaspan, T., Roberts, N., Blumhardt, L.D., 1999. Infratentorial atrophy on magnetic resonance imaging and disability in multiple sclerosis. Brain 122 (Pt 2), 291–301.

Erturk, A., Bradke, F., 2013. High-resolution imaging of entire organs by 3-dimensional imaging of solvent cleared organs (3DISCO). Exp. Neurol. 242, 57–64.

Erturk, A., Hellal, F., Enes, J., Bradke, F., 2007. Disorganized microtubules underlie the formation of retraction bulbs and the failure of axonal regeneration. J. Neurosci. 27, 9169–9180.

Erturk, A., Becker, K., Jahrling, N., Mauch, C.P., Hojer, C.D., Egen, J.G., Hellal, F., Bradke, F., Sheng, M., Dodt, H.U., 2012a. Three-dimensional imaging of solvent-cleared organs using 3DISCO. Nat. Protoc. 7, 1983–1995.

Erturk, A., Mauch, C.P., Hellal, F., Forstner, F., Keck, T., Becker, K., Jahrling, N., Steffens, H., Richter, M., Hubener, M., Kramer, E., Kirchhoff, F., Dodt, H.U., Bradke, F., 2012b. Three-dimensional imaging of the unsectioned adult spinal cord to assess axon regeneration and glial responses after injury. Nat. Med. 18, 166–171.

Ferguson, B., Matyszak, M.K., Esiri, M.M., Perry, V.H., 1997. Axonal damage in acute multiple sclerosis lesions. Brain 120 (Pt 3), 393–399.

Fisher, E., Rudick, R.A., Simon, J.H., Cutter, G., Baier, M., Lee, J.C., Miller, D., Weinstock-Guttman, B., Mass, M.K., Dougherty, D.S., Simonian, N.A., 2002. Eight-year follow-up study of brain atrophy in patients with MS. Neurology 59, 1412–1420.

Franklin, K.B.J., Paxinos, G., 2008. The Mouse Brain in Stereotaxic Coordinates, 3rd ed. Academic Press, New York.

Gold, S.M., Voskuhl, R.R., 2009. Estrogen treatment in multiple sclerosis. J. Neurol. Sci. 286, 99–103.

Hama, H., Kurokawa, H., Kawano, H., Ando, R., Shimogori, T., Noda, H., Fukami, K., Sakaue-Sawano, A., Miyawaki, A., 2011. Scale: a chemical approach for fluorescence imaging and reconstruction of transparent mouse brain. Nat. Neurosci. 14, 1481–1488.

Iannucci, G., Minicucci, L., Rodegher, M., Sormani, M.P., Comi, G., Filippi, M., 1999. Correlations between clinical and MRI involvement in multiple sclerosis: assessment using T(1), T(2) and MT histograms. J. Neurol. Sci. 171, 121–129.

Imitola, J., Cote, D., Rasmussen, S., Xie, X.S., Liu, Y., Chitnis, T., Sidman, R.L., Lin, C.P., Khoury, S.J., 2011. Multimodal coherent anti-Stokes Raman scattering microscopy reveals microglia-associated myelin and axonal dysfunction in multiple sclerosis-like lesions in mice. J. Biomed. Opt. 16, 021109.

Ke, M.T., Fujimoto, S., Imai, T., 2013. SeeDB: a simple and morphology-preserving optical clearing agent for neuronal circuit reconstruction. Nat. Neurosci. 16, 1154–1161.

Koo, E.H., Sisodia, S.S., Archer, D.R., Martin, L.J., Weidemann, A., Beyreuther, K., Fischer, P., Masters, C.L., Price, D.L., 1990. Precursor of amyloid protein in Alzheimer disease

undergoes fast anterograde axonal transport. Proc. Natl. Acad. Sci. U. S. A. 87, 1561–1565.
Kovacevic, N., Henderson, J.T., Chan, E., Lifshitz, N., Bishop, J., Evans, A.C., Henkelman, R.M., Chen, X.J., 2005. A three-dimensional MRI atlas of the mouse brain with estimates of the average and variability. Cereb. Cortex 15, 639–645.
Lau, J.C., Lerch, J.P., Sled, J.G., Henkelman, R.M., Evans, A.C., Bedell, B.J., 2008. Longitudinal neuroanatomical changes determined by deformation-based morphometry in a mouse model of Alzheimer's disease. Neuroimage 42, 19–27.
Liu, H.B., Loo, K.K., Palaszynski, K., Ashouri, J., Lubahn, D.B., Voskuhl, R.R., 2003. Estrogen receptor alpha mediates estrogen's immune protection in autoimmune disease. J. Immunol. 171, 6936–6940.
Lovas, G., Szilagyi, N., Majtenyi, K., Palkovits, M., Komoly, S., 2000. Axonal changes in chronic demyelinated cervical spinal cord plaques. Brain 123 (Pt 2), 308–317.
MacKenzie-Graham, A., Lee, E.F., Dinov, I.D., Bota, M., Shattuck, D.W., Ruffins, S., Yuan, H., Konstantinidis, F., Pitiot, A., Ding, Y., Hu, G., Jacobs, R.E., Toga, A.W., 2004. A multimodal, multidimensional atlas of the C57BL/6 J mouse brain. J. Anat. 204, 93–102.
MacKenzie-Graham, A., Tiwari-Woodruff, S.K., Sharma, G., Aguilar, C., Vo, K.T., Strickland, L.V., Morales, L., Fubara, B., Martin, M., Jacobs, R.E., Johnson, G.A., Toga, A.W., Voskuhl, R.R., 2009. Purkinje cell loss in experimental autoimmune encephalomyelitis. Neuroimage 48, 637–651.
MacKenzie-Graham, A., Rinek, G.A., Avedisian, A., Gold, S.M., Frew, A.J., Aguilar, C., Lin, D.R., Umeda, E., Voskuhl, R.R., Alger, J.R., 2012. Cortical atrophy in experimental autoimmune encephalomyelitis: in vivo imaging. Neuroimage 60, 95–104.
Mangiardi, M., Crawford, D.K., Xia, X., Du, S., Simon-Freeman, R., Voskuhl, R.R., Tiwari-Woodruff, S.K., 2011. An animal model of cortical and callosal pathology in multiple sclerosis. Brain Pathol. 21, 263–278.
Nikic, I., Merkler, D., Sorbara, C., Brinkoetter, M., Kreutzfeldt, M., Bareyre, F.M., Bruck, W., Bishop, D., Misgeld, T., Kerschensteiner, M., 2011. A reversible form of axon damage in experimental autoimmune encephalomyelitis and multiple sclerosis. Nat. Med. 17, 495–499.
Pender, M.P., 1987. Demyelination and neurological signs in experimental allergic encephalomyelitis. J. Neuroimmunol. 15, 11–24.
Peterson, J.W., Bo, L., Mork, S., Chang, A., Trapp, B.D., 2001. Transected neurites, apoptotic neurons, and reduced inflammation in cortical multiple sclerosis lesions. Ann. Neurol. 50, 389–400.
Pettinelli, C.B., McFarlin, D.E., 1981. Adoptive transfer of experimental allergic encephalomyelitis in SJL/J mice after in vitro activation of lymph node cells by myelin basic protein: requirement for Lyt 1 + 2- T lymphocytes. J. Immunol. 127, 1420–1423.
Pirko, I., Lucchinetti, C.F., Sriram, S., Bakshi, R., 2007. Gray matter involvement in multiple sclerosis. Neurology 68, 634–642.
Porrero, C., Rubio-Garrido, P., Avendano, C., Clasca, F., 2010. Mapping of fluorescent protein-expressing neurons and axon pathways in adult and developing Thy1-eYFP-H transgenic mice. Brain Res. 1345, 59–72.
Rex, D.E., Ma, J.Q., Toga, A.W., 2003. The LONI pipeline processing environment. Neuroimage 19, 1033–1048.
Rudick, R.A., Trapp, B.D., 2009. Gray-matter injury in multiple sclerosis. N. Engl. J. Med. 361, 1505–1506.
Sailer, M., Fischl, B., Salat, D., Tempelmann, C., Schonfeld, M.A., Busa, E., Bodammer, N., Heinze, H.J., Dale, A., 2003. Focal thinning of the cerebral cortex in multiple sclerosis. Brain 126, 1734–1744.
Sanfilipo, M.P., Benedict, R.H., Weinstock-Guttman, B., Bakshi, R., 2006. Gray and white matter brain atrophy and neuropsychological impairment in multiple sclerosis. Neurology 66, 685–692.
Shattuck, D.W., Leahy, R.M., 2001. Automated graph-based analysis and correction of cortical volume topology. IEEE Trans. Med. Imaging 20, 1167–1177.
Sherriff, F.E., Bridges, L.R., Gentleman, S.M., Sivaloganathan, S., Wilson, S., 1994. Markers of axonal injury in post mortem human brain. Acta Neuropathol. 88, 433–439.
Shriver, L.P., Dittel, B.N., 2006. T-cell-mediated disruption of the neuronal microtubule network: correlation with early reversible axonal dysfunction in acute experimental autoimmune encephalomyelitis. Am. J. Pathol. 169, 999–1011.
Suen, W.E., Bergman, C.M., Hjelmstrom, P., Ruddle, N.H., 1997. A critical role for lymphotoxin in experimental allergic encephalomyelitis. J. Exp. Med. 186, 1233–1240.
Susaki, E.A., Tainaka, K., Perrin, D., Kishino, F., Tawara, T., Watanabe, T.M., Yokoyama, C., Onoe, H., Eguchi, M., Yamaguchi, S., Abe, T., Kiyonari, H., Shimizu, Y., Miyawaki, A., Yokota, H., Ueda, H.R., 2014. Whole-brain imaging with single-cell resolution using chemical cocktails and computational analysis. Cell 157, 726–739.
Tomer, R., Ye, L., Hsueh, B., Deisseroth, K., 2014. Advanced CLARITY for rapid and high-resolution imaging of intact tissues. Nat. Protoc. 9, 1682–1697.
Trapp, B.D., Peterson, J., Ransohoff, R.M., Rudick, R., Mork, S., Bo, L., 1998. Axonal transection in the lesions of multiple sclerosis. N. Engl. J. Med. 338, 278–285.
van den Elskamp, I.J., Boden, B., Dattola, V., Knol, D.L., Filippi, M., Kappos, L., Fazekas, F., Wagner, K., Pohl, C., Sandbrink, R., Polman, C.H., Uitdehaag, B.M., Barkhof, F., 2010. Cerebral atrophy as outcome measure in short-term phase 2 clinical trials in multiple sclerosis. Neuroradiology 52, 875–881.
Vigeveno, R.M., Wiebenga, O.T., Wattjes, M.P., Geurts, J.J., Barkhof, F., 2012. Shifting imaging targets in multiple sclerosis: from inflammation to neurodegeneration. J. Magn. Reson. Imaging 36, 1–19.
Woods, R.P., Grafton, S.T., Holmes, C.J., Cherry, S.R., Mazziotta, J.C., 1998a. Automated image registration: I. General methods and intrasubject, intramodality validation. J. Comput. Assist. Tomogr. V22, 139–152.
Woods, R.P., Grafton, S.T., Watson, J.D., Sicotte, N.L., Mazziotta, J.C., 1998b. Automated image registration: II. Intersubject validation of linear and nonlinear models. J. Comput. Assist. Tomogr. 22, 153–165.
Wujek, J.R., Bjartmar, C., Richer, E., Ransohoff, R.M., Yu, M., Tuohy, V.K., Trapp, B.D., 2002. Axon loss in the spinal cord determines permanent neurological disability in an animal model of multiple sclerosis. J. Neuropathol. Exp. Neurol. 61, 23–32.
Zhang, J., Peng, Q., Li, Q., Jahanshad, N., Hou, Z., Jiang, M., Masuda, N., Langbehn, D.R., Miller, M.I., Mori, S., Ross, C.A., Duan, W., 2010. Longitudinal characterization of brain atrophy of a Huntington's disease mouse model by automated morphological analyses of magnetic resonance images. Neuroimage 49, 2340–2351.
Zhu, B., Luo, L., Moore, G.R., Paty, D.W., Cynader, M.S., 2003. Dendritic and synaptic pathology in experimental autoimmune encephalomyelitis. Am. J. Pathol. 162, 1639–1650.
Ziehn, M.O., Avedisian, A.A., Tiwari-Woodruff, S., Voskuhl, R.R., 2010. Hippocampal CA1 atrophy and synaptic loss during experimental autoimmune encephalomyelitis, EAE. Lab. Invest. 90, 774–786.

Please cite this article as: Spence, R.D., et al., Bringing CLARITY to gray matter atrophy, NeuroImage (2014), http://dx.doi.org/10.1016/j.neuroimage.2014.07.017